Stability Analysis of Retrofitted Thin-Walled Slender Columns Subjected to Edge Loads using Finite Element Method

T Rajanna [1*], P.K Ravindra[2], G Venkataramaiah[3], S Manjunatha[4] and Imran Khan[5]

[1*] Associate Professor, t.rajanna@gmail.com, B.M.S. College of Engineering, Bengaluru 560019, India

[2] Associate Professor, ravindrapkravindra@ymail.com, Government Engineering College Ramanagara 562159, India

[3] Associate Professor, gvr66ramaiah@gmail.com, Government Engineering College Ramanagara 562159, India

[4] Associate Professor, manjunathswamy67@gmail.com, Government S.K.S.J.T.I, Bengaluru 560001, India

[5] Associate Professor, imrangce@gmail.com, Government Engineering College Ramanagara 562159, India

***Abstract*:**

In modern high-rise construction, thin-walled slender columns are commonly used due to their structural efficiency and aesthetic appearance. These columns often require retrofitting using Fibre-Reinforced Polymer (FRP) laminates to enhance their load-carrying capacity or to strengthen existing structures. The present investigation examines the stability behaviour of such columns, both with and without FRP retrofitting, when subjected to partial or concentrated edge loads. The analysis is carried out using a finite element (FE) formulation that incorporates shear deformation and rotary inertia effects. The column is discretized using an eight-noded plate element, with five degrees of freedom per node. This study primarily focuses on understanding the influence of different ply orientations in the retrofitted FRP laminates, positioning of partial/concentrated loads, and number of stories (height effect) on the stability performance of the thin-walled slender columns.

Keywords: Buckling, thin-walled columns, finite element method, FRP retrofitting.

1. Introduction:

Rapid advancements in material science and structural engineering have enabled the development of slender and efficient structural members, particularly in high-rise construction. Among these, thin-walled reinforced concrete (RC) columns have gained prominence due to their optimized use of material and increased permissible stress levels. However, despite their advantages, such columns are prone to stability failures—such as buckling—long before reaching their material strength limits. This has shifted the focus of structural analysis from traditional strength-based approaches to those emphasizing stability considerations. In the rehabilitation and upgrading of aging or damaged columns, Fiber-Reinforced Polymer (FRP) composites have emerged as a reliable retrofitting solution due to their high strength-to-weight ratio, corrosion resistance, and ease of application. A significant body of work has focused on the performance of FRP-wrapped or laminated RC columns, particularly under concentric loads. Experimental and numerical studies have demonstrated improvements in strength and ductility by varying laminate types, sizes, and configurations [1–3]. Common techniques include externally bonded FRP fabrics, bars, and laminates. For instance, Hussein et al. [4] studied the impact of wrapping size on circular RC columns and found minimal discrepancies between experimental and numerical results. However, the stress behavior in non-circular cross sections remains complex and underexplored. Addressing eccentric loading, Hadi [5] evaluated CFRP-confined RC columns and observed enhanced load capacity and ductility, alongside improved moment redistribution. Similarly, Belouar et al. [6] showed that while increasing the number of CFRP layers improves compressive strength, greater slenderness ratios reduce ductility. On the modeling front, Charalambidi et al. [7] used finite element analysis with 8-noded elements to simulate partial GFRP confinement of low-strength concrete columns. Meanwhile, internal retrofitting approaches using FRP spirals and longitudinal bars were studied by Hales et al. [8], who found that these reinforcements significantly enhance tensile capacity and overall load resistance. The lack of existing design guidelines for slender FRP-

confined columns has prompted theoretical work. Jiang and Teng [9] developed a numerical integration-based model using Lam and Teng's stress–strain relations. Their predictions aligned well with experimental data, but the authors emphasized the need for further large-scale testing to enhance the model's robustness. Expanding on hybrid systems, Chellapandian et al. [10] explored RC columns strengthened with both CFRP laminates and external fabrics under axial and eccentric loads. Using experimental, analytical, and finite element (FE) approaches, their study confirmed that hybrid retrofitting significantly improved initial stiffness, peak load, and ductility. FE and analytical predictions were within 5% of test results, confirming their validity. Similarly, Mosallam [11] investigated FRP-retrofitted RC beam-column joints using high-strength and high-modulus carbon/epoxy laminates, as well as hybrid composite connectors. These systems improved structural performance under full cyclic and gravity loads with good agreement between experimental and numerical outcomes.From a plate-theory perspective, Sahu et al. [12] analyzed laminated plates under buckling using varied ply orientations—symmetric and antisymmetric—to understand load interaction effects. In a related study, Nali and Carrera [13] investigated the mechanical response of orthotropic and anisotropic laminated composites with different stacking sequences, further contributing to the understanding of composite behavior under complex loads.

Despite these substantial efforts, most existing research focuses on square or circular RC columns under concentric loading. The buckling behavior of thin-walled slender RC columns retrofitted with FRP under eccentric or partial edge loading conditions remains largely unaddressed. Given the importance of such columns in modern structural systems, a detailed parametric study is essential. This research addresses this gap by examining the effects of FRP retrofitting, ply orientation, eccentric load positioning, column height, and boundary constraints on the stability behavior of thin-walled slender columns. The study offers a comprehensive evaluation under varying load scenarios to enhance the understanding and design of retrofitted slender RC columns.

2. Thin-Walled Slender Columns and Influence of Loading Position.

Thin-walled slender columns are structural elements characterized by relatively small cross-sectional dimensions in relation to their length, often leading to stability concerns under axial or eccentric loads. In such columns, the ultimate load-bearing capacity is not determined solely by the material strength and cross-sectional area but is significantly affected by their slenderness ratio. Figures 1(a) and 1(b) illustrate the slender nature of these thin-walled columns. Compared to short or stocky columns, slender columns—especially those with thin walls—exhibit reduced axial load capacity as their length increases, making them more sensitive to buckling and load positioning.

(a) (b)

Fig 1: (a)-(b) Thin walled slender columns

The typical partial in-plane edge loading and concentrated loading cases that are considered in the following investigations are shown in Fig 2 (a) – (d) respectively. The original pre-buckling stresses are determined where the column's load (P) remain constant irrespective of the length of the localized edge load. These localized edge loading in Fig 2 (a) – (d) are compressive in nature. In these localized edge loading, the parameter 'c' defines the width of loading, 'b' defines the width of the column. When c/b = 1 the column becomes uniformly loaded for loading cases as specified above.

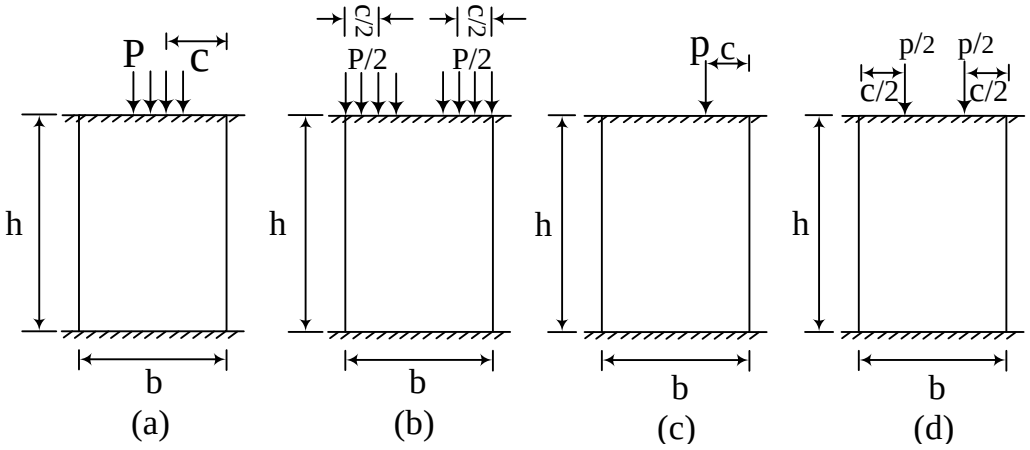

Fig 2: Problem description: Partial edge loading (a) from one end, (b) from both ends and Point load (c) from one end, (d) from both ends.

3. Finite element formulation and governing equations

A typical plate, as illustrated in Fig. 3, has dimensions a × b × h along the x, y, and z axes, respectively. The plate is composed of a unidirectional composite fiber laminate. To derive the expression for strain energy, five independent displacement coordinates are considered: u, v, and w, representing displacements along the x, y, and z directions, and Θ_x and Θ_y, representing rotations about the y and x axes, respectively. These displacement components form the basis for analyzing the plate's deformation behavior under loading.

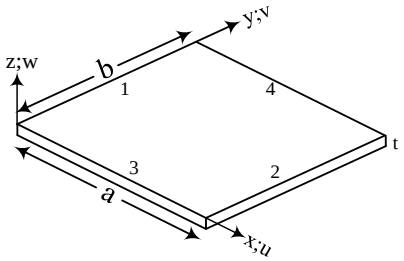

Fig 3: Lamina geometry of plate

The First-order Shear Deformation Theory (FSDT) is employed, incorporating a shear correction factor to account for the non-linear shear strain distribution through the thickness. The displacement field assumes that normals to the mid-surface remain straight but not necessarily perpendicular after deformation, such that

$$\left\{\bar{u}^p(x,y,z),\ \bar{v}^p(x,y,z),\ \bar{w}^p(x,y,z)\right\} = \left\{u^p(x,y),\ v^p(x,y),\ w^p(x,y)\right\} + z\left\{\theta_x^p(x,y),\ \theta_y^p(x,y),\ 0\right\} \quad (1)$$

where $\bar{u}^p$,$\bar{v}^{pi}$and $\bar{w}^p$represent the displacements in the x, y, and z directions,while u^p, v^p, and w^pdenotemid-plane displacements along x, y, and z axes. Additionally,θ_x^p and θ_y^pindicate rotations of the normalto the un-deformed mid-plane of the plate about the y and x-axes, respectively. In the current formulation, Eq. (2) presents the Green-Lagrange's strain displacement relation for a plate element.

$$\left.\begin{aligned}
\varepsilon_{xp} &= \left(\frac{\partial \overline{u}^{p}}{\partial x}\right)+\frac{1}{2}\left(\frac{\partial u^{p}}{\partial x}\right)^{2}+\frac{1}{2}\left(\frac{\partial v^{p}}{\partial x}\right)^{2}+\frac{1}{2}\left(\frac{\partial w^{p}}{\partial x}\right)^{2}+\frac{1}{2}z^{2}\left[\left(\frac{\partial \theta_{x}^{p}}{\partial x}\right)^{2}+\left(\frac{\partial \theta_{y}^{p}}{\partial x}\right)^{2}\right] \\
\varepsilon_{yp} &= \left(\frac{\partial \overline{v}^{p}}{\partial y}\right)+\frac{1}{2}\left(\frac{\partial u^{p}}{\partial y}\right)^{2}+\frac{1}{2}\left(\frac{\partial v^{p}}{\partial y}\right)^{2}+\frac{1}{2}\left(\frac{\partial w^{p}}{\partial y}\right)^{2}+\frac{1}{2}z^{2}\left[\left(\frac{\partial \theta_{x}^{p}}{\partial y}\right)^{2}+\left(\frac{\partial \theta_{y}^{p}}{\partial y}\right)^{2}\right] \\
\gamma_{xyp} &= \left(\frac{\partial \overline{u}^{p}}{\partial y}+\frac{\partial \overline{v}^{p}}{\partial x}\right)+\frac{\partial u^{p}}{\partial x}\frac{\partial u^{p}}{\partial y}+\frac{\partial v^{p}}{\partial x}\frac{\partial v^{p}}{\partial y}+\left(\frac{\partial w^{p}}{\partial x}\right)\left(\frac{\partial w^{p}}{\partial y}\right)+z^{2}\left[\frac{\partial \theta_{x}^{p}}{\partial x}\frac{\partial \theta_{x}^{p}}{\partial y}+\frac{\partial \theta_{y}^{p}}{\partial x}\frac{\partial \theta_{y}^{p}}{\partial y}\right]
\end{aligned}\right\} \quad (2)$$

The strain-displacement equation, which is shown in Eq. (2) has two parts, i.e., linear strain and non-linear strains,

$$\left\{\varepsilon_{ij}\right\} = \left\{\varepsilon_{ij}^{L}\right\} + \left\{\varepsilon_{ij}^{NL}\right\} \quad (3)$$

The linear strain vector $\{\varepsilon_{ij}^{L}\}$ is employed for the elastic stiffness matrix, and the non-linear strain term $\{\varepsilon_{ij}^{NL}\}$ is used for the geometric stiffness matrix. Under the assumption of minimal and neglected normal stresses, the stress-strain relation for the laminated panel is derived based on the displacement model as,

$$\begin{Bmatrix} N_x^p \\ N_y^p \\ N_{xy}^p \\ M_x^p \\ M_y^p \\ M_{xy}^p \\ Q_{xz}^p \\ Q_{yz}^p \end{Bmatrix} = \begin{bmatrix} A_{11}^p & A_{12}^p & A_{16}^p & B_{11}^p & B_{12}^p & B_{16}^p & 0 & 0 \\ A_{12}^p & A_{22}^p & A_{26}^p & B_{12}^p & B_{22}^p & B_{26}^p & 0 & 0 \\ A_{16}^p & A_{26}^p & A_{66}^p & B_{16}^p & B_{26}^p & B_{66}^p & 0 & 0 \\ B_{11}^p & B_{12}^p & B_{16}^p & D_{11}^p & D_{12}^p & D_{16}^p & 0 & 0 \\ B_{12}^p & B_{22}^p & B_{26}^p & D_{12}^p & D_{22}^p & D_{26}^p & 0 & 0 \\ B_{16}^p & B_{26}^p & B_{66}^p & D_{16}^p & D_{26}^p & D_{66}^p & 0 & 0 \\ 0 & 0 & 0 & 0 & 0 & 0 & S_{44}^p & S_{45}^p \\ 0 & 0 & 0 & 0 & 0 & 0 & S_{45}^p & S_{55}^p \end{bmatrix} \begin{Bmatrix} u_{,x}^p \\ v_{,y}^p \\ u_{,y}^p + v_{,x}^p \\ \theta_{x,x}^p \\ \theta_{y,y}^p \\ \theta_{x,y}^p + \theta_{y,x}^p \\ w_{,x}^p + \theta_{\mathrm{xp}} \\ w_{,y}^p + \theta_{\mathrm{yp}} \end{Bmatrix} \quad (4)$$

where the comma subscript denotes differentiation with respect to the coordinates following the subscript.

The laminates constitutive coefficients in Eq. (4) are defined by,

$$(A_{ij}^P,\ B_{ij}^P,\ D_{ij}^P) = \sum_{k=1}^{m}\int_{z_{k-1}}^{z_k}\left(\overline{Q}_{ij}^{p}\right)(1,\ z,\ z^2)\ dz \quad \text{for i, j= 1, 2, 6} \quad (5)$$

whereas the shear component is indicated by $S_{ij}^P = \sum_{k=1}^{m}\int_{z_{k-1}}^{z_k}\kappa^p\left(\overline{Q}_{ij}^{p}\right)dz$ for i, j= 4,5 (6)

Here κ^p is the shear correction factor, which is used to compensate for the parabolic shear stress distribution across the plate thickness and is taken to be 5/6.

The linear and non-linear strain terms in Eq (2) and resultant stress-strain relations in Eq. (4) are used to derive the different level stiffness matrices as follows:

$$\left[k_e^p\right] = \int_{-1}^{1}\int_{-1}^{1}\left[B^p\right]^T\left[D^P\right]\left[B^p\right]\left|J^p\right|d\xi d\eta \quad (7)$$

$$\left[k_G^p\right] = \int_{-1}^{1}\int_{-1}^{1}\left[B_G^p\right]^T\left[S^P\right]\left[B_G^p\right]\left|J^p\right|d\xi d\eta \quad (8)$$

$$\left[m^p\right] = \int_{-1}^{+1}\int_{-1}^{+1}\left[\overline{N}^p\right]^T\left[\overline{I}^p\right]\left[\overline{N}^p\right]\left|J^p\right|d\xi d\eta \quad (9)$$

where $\left[k_e^p\right]$, $\left[k_G^p\right]$ and $\left[m^p\right]$ represents element level stiffness, geometric stiffness and mass matrices, respectively. Structural stiffness matrices are assembled from individual element-level matrices using the skyline technique.

The governing differential equation of equilibrium for a structural component under the application of in-plane edge load can be obtained by using extended Hamilton's principle as,

$$\left[\mathrm{M}\right]\{\ddot{\mathrm{q}}\} + \left[\left[\mathrm{K}\right] - \mathrm{P}_0\left[\mathrm{K}_\mathrm{G}\right]\right]\{\mathrm{q}\} = \{0\} \quad (10)$$

The assembled matrices [K], [K_G], and [M] represent system elastic stiffness, geometric stiffness, and mass, respectively. Equation (10) can be simplified for buckling and vibration scenarios.

In the case of buckling, when$\{\ddot{q}\}$=0, the equationreduces to:

$$\left[\mathrm{K}\right]\{\mathrm{q}\} - \mathrm{P}_{\mathrm{cr}}\left[\mathrm{K}_\mathrm{G}\right]\{\mathrm{q}\} = \{0\} \quad (11)$$

In the case of vibration, equation (10) becomes,

$$\left[\mathrm{K}\right]\{\mathrm{q}\} - \mathrm{P}_0\left[\mathrm{K}_\mathrm{G}\right]\{\mathrm{q}\} - \omega^2\left[\mathrm{M}\right]\{\mathrm{q}\} = \{0\}. \quad (12)$$

In Eq. (12), when P_0 approaches zero, the equation describes free vibration without in-plane load, while the presence of P_0 signifies a vibration problem with in-plane load effects. Setting ω^2 to zero in Eq. (12) for a specific P_0 value identifies the critical buckling load. This dynamic approach to determine critical loads is advantageous as it circumvents singularity issues posed by Eigen value solvers in static analysis. This method has been applied to ascertain critical loads for diverse problems in the study.

4. PROBLEM DEFINITIONS

Buckling responses of a retrofitted thin-walled column under various in-plane edge loading conditions (Fig. 2) are presented. The stress–strain relationships, engineering constants, and failure theories for an angle lamina have been established and serve as key parameters for evaluation. Unlike isotropic materials, determining these parameters experimentally for composites is time-consuming and costly due to dependencies on constituent properties, volume fraction, geometry, and

processing. When the material symmetry aligns with the fiber direction, five independent elastic constants are needed to describe the elastic behavior.

Numerous analytical models have been developed to estimate these constants by relating fiber and matrix properties. These models, based on different experimental data and assumptions, are well-documented in the works of Whitney and Riley [16], Halpin and Tsai [17], Selvadurai and Nikopour [18], and Hashin and Rosen [19].

Table 1: Isotropic properties of concrete and steel

Particulars		Concrete
Young's modulus	E_c	25000 MPa
Shear modulus	G_c	10869.5 MPa
Poisson's value	ϑ_c	0.15
Density	ρ_c	2400 Kg/m^3

Particulars		Steel
Young's modulus	E_s	200000 MPa
Shear modulus	G_s	76869.5 MPa
Poisson's value	ϑ_s	0.30
Density	ρ_s	7850 Kg/m^3

Table 2: Calculated concrete equivalent young's modulus for varying % of steel

Sl. No	Particulars	Percentage of steel (Volume fraction Vs)				
		0.8	1	2	2.5	3
1.	**Longitudinal Direction(E_{11}) (N/mm^2)**					
a.	Rule of mixture	26400.00	26750.00	28500.00	29375.00	30250.00
b.	MROM	26400.00	26750.00	28500.00	29375.00	30250.00
c.	Chamis method	26400.00	26750.00	28500.00	29375.00	30250.00
d.	Elasticity approach	26407.10	26759.11	28517.93	29397.23	30276.40
2.	**Transverse Direction(E_{22}) (N/mm^2)**					
a.	Inverse rule of mixture	25176.20	25220.60	25445.90	25559.11	25673.90
b.	MROM	25338.80	25421.93	25829.46	26028.80	26225.60
c.	Chamis method	31377.90	31746.03	33277.59	33937.40	34556.80
d.	Halpin– Tsai [17]	25201.10	25252.53	25510.20	25641.03	25773.20
3.	**Rigidity Shear Modulus (G_{12}= G_{13} and G_{23}) (N/mm^2)**					
a.	Rule of mixture	10944.70	10963.71	11059.50	11108.03	11156.90
b.	MROM	10994.70	11026.32	11185.52	11266.04	11347.20
c.	Chamis method	13901.60	14064.70	14743.24	15035.56	15310.00
d.	Elasticity approach	11001.20	11034.37	11201.68	11286.31	11371.80

e.	Rule of mixture (G_{23})	11005.30	11038.61	11200.98	11280.08	11358.00
4.	**ϑ value (ϑ_{12})**					
a.	Rule of mixture	0.1512	0.1515	0.153	0.1537	0.1545
b.	elasticity approach	0.1519	0.1523	0.1547	0.1559	0.1571

The above mentioned Table 2 provides the young's modulus of RCC by assigning the properties of concrete and steel specifically, for different percentage of steel varying from 0.8% to 3.0%.

Table 3: Geometric boundary conditions

Boundary condition		Position of the edge	
		y = 0 (bottom)	y = b (top)
Simply supported (S)		x = 0, w = 0, $\theta_y = 0$	w = 0, $\theta_y = 0$
Clamped (C)	BC-1	x = 0, y = 0, w = 0, $\theta_x = 0$, $\theta_y = 0$	x = 0, w = 0, $\theta_x = 0$, $\theta_y = 0$
	BC-2	x = 0, y = 0, w = 0, $\theta_x = 0$, $\theta_y = 0$	x = 0, $\theta_x = 0$, $\theta_y = 0$
Free (F)		No restraints	

The present investigation in mainly focused on the slender concrete column with retrofitting. First the isotropic properties of concrete and steel are used to calculate the orthotropic properties of the RCC by considering it as composite material and the properties of the retrofitting material is selected from Kishore et al. [15] as mentioned in table 4.

Table 4: Material properties of slender column for 2% steel and epoxy/carbon laminate.

Material	Material constants					
	E_{11}	E_{12}	G_{12}	G_{13}	G_{23}	ν_{12}
RC Column	28.54e3	25.82e3	11.20e3	11.20e3	11.20e3	0.153
Carbon/epoxy	172.5e3	6.9e3	3.5e3	3.5e3	1.4e3	0.25

5. RESULTS AND DISCUSSIONS

Convergence studies

For adequate convergence conditions, it is vital to properly discretize the structure in the finite element method. In this respect, the column is discretized in m, row number and n, columns, i.e. m x n column elements and the respective values are shown in Table 5. The ratio of local width c/b = 0.5. Results convergence is observed to be satisfactory for 20 x 10 mesh sizes as observed in Table 5. This mesh size is therefore retained based on the loading throughout the work.

Table 5: Convergence of buckling load (γ_{cr}) for CC edge partial load for c/b = 0.5

Mesh order, m x n	$[\pm 0]_s$/RCC/$[\pm 0]_s$	$[\pm 90]_s$/RCC/$[\pm 90]_s$
4 x 2	3.775×10^4	5.332×10^4

8 x 4	3.764×10^4	5.236×10^4
12 x 6	3.695×10^4	5.165×10^4
16 x 8	3.601×10^4	5.095×10^4
20 x 10	3.512×10^4	5.068×10^4
24 x 12	3.512×10^4	5.068×10^4

Comparison studies

Comparison studies are needed to determine the precision and effectiveness of various matrices and in discretization of the structure engaged in buckling problems. In order to validate the accuracy of the computed stiffness matrix, buckling analysis of a square laminated plate is predicted using an 8-noded serendipity element (8-NSE) and compared with the closed forms solutions of Sahu et al. [12] as shown in table 6.

Table 6: Non-dimensional buckling load comparison for simply supported loads between current finite element methods.($W = P_{cr}*b^2 / E_{22}*h^3$) a/b = 1, E_{11}/E_{22} = 25, $G_{12} = G_{13} = 0.5E_{22}$, $G_{23} = 0.1E_{22}$ and v_{12} = 0.25.

C/b ratio	Particulars	Ply-orientation [θ/- θ/ θ/- θ]					
		0	15	30	45	60	90
0.2	Sahu et al. [12]	70.5	73.4	76.6	35.25	19.65	14.91
	Present values	70.13	73.05	76.41	35.01	19.58	14.77
0.6	Sahu et al. [12]	34.68	39.98	49.76	35.25	25.78	13.01
	Present values	33.68	39.63	49.04	35.03	25.52	12.84
1.0	Sahu et al. [12]	23.37	25.21	32.03	35.78	29.59	10.45
	Present values	23.07	24.97	31.84	35.21	29.16	10.22

6. Buckling analysis of column with retrofitting

By considering various parameters, the buckling analysis of the column with retrofitting under the application of different partial and concentrated positioning in plane edge load (c/b) is studied such as variation in loading position, height of column, constrain position, storey constrain position and different boundary condition. A 4-layered laminate of 2mm thick symmetrically stacked is considered on each face of the column, $(\pm\Theta)_S$. The load applied on the column is considered to be of constant intensity for partial and concentrated load i.e. for partial load and concentrated load of P=1000N is considered. The characteristics strength of concrete is taken as M25 and dimensions of column are Height (h) = 3000 mm, width (b) = 1000 mm, thickness (t) = 150 mm.

6.1 Effect of position of partial edge load.

The effect of load position ratio (c/b) for column subjected to partial load from one and both edge on the buckling behaviour of fixed-fixed (C-C) column retrofitted with different ply-oriented laminate of carbon/epoxy with a thickness of 2mm on each face of column is shown in Fig. 4 (a) and Fig 4 (b). The partial load width is kept constant as 200 mm and its position is changing from c/b = 0.1 to 0.5. It is observed from Fig 4(a) that the buckling load increases with the increase in load position ratio (c/b) up o c/b = 0.5 irrespective of ply-orientation.

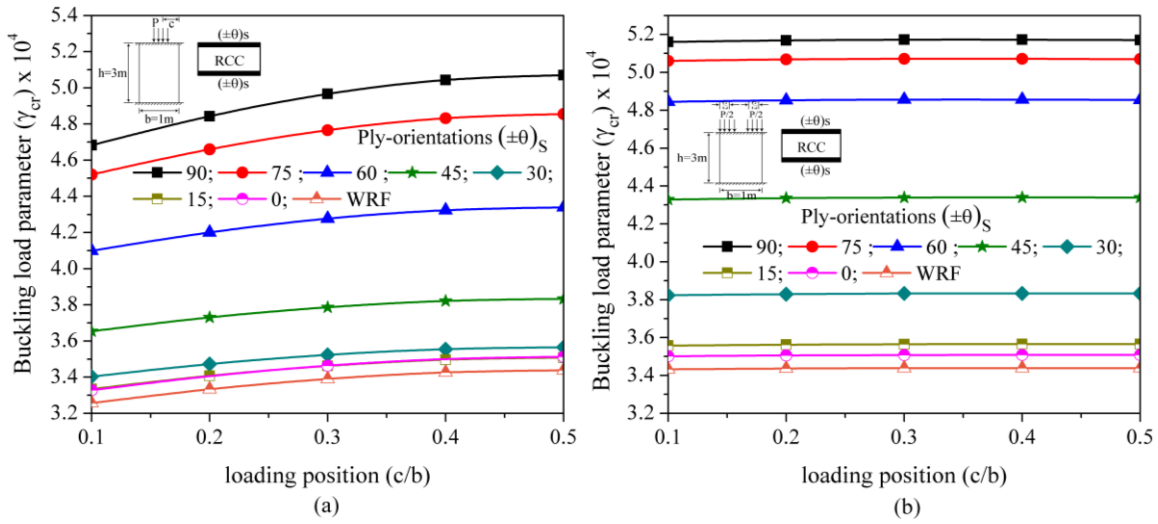

Fig 4: Variation of buckling load (γ_{cr}) with the position of (a) partial load from one edge (b) partial load from both edges.

It is worth to mention that the buckling load is found to be maximum at c/b = 0.5 and it is found to be minimum when c/b = 0.1. But where as in Fig 4(b) the critical buckling load does not vary much for different c/b ratio irrespective of ply-orientation. It is also observed that the buckling load increases with the increases in ply-orientation and found to be maximum at $\theta = (\pm 90°)_S$ and minimum at $\theta = (\pm 15°)_S$ or $(\pm 0°)_S$ irrespective of position of load and edges. It may be attributed to the fact that the fibre contribution towards the buckling resistance is predominant when $\theta = (\pm 90°)_S$ and it decreases as the ply-orientation decreases and the fibre contribution becomes almost negligible when $\theta = (\pm 0°)_S$.

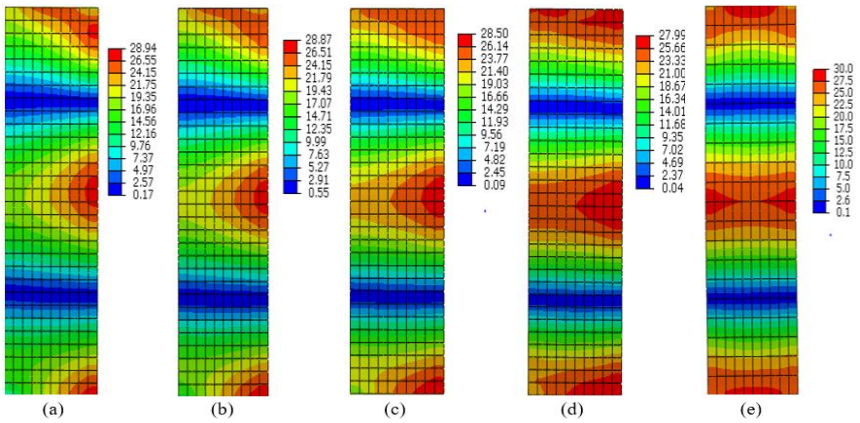

Fig. 5: Stress distributiom for partial load from one edge for $\theta = (\pm 90°)_S$: (a) c/b = 0.1, (b) c/b = 0.2, (c) c/b = 0.3, (d) c/b = 0.4, (e) c/b = 0.5.

The buckling behaviour of panel is dependent on the various parameters, in which pre-buckling stress distribution plays an important role, as the pre-buckling stress depends on the parameters like nature of loading, loading position, ply-orientation and boundary condition. Retrofitted slender columns are subjected to non-uniform loading that may develop non-uniform stress for columns with different ply-orientation. Hence, it becomes necessary to study the nature of in-plane stress distribution for non-uniform edge loads as in Fig 5 and Fig 6.

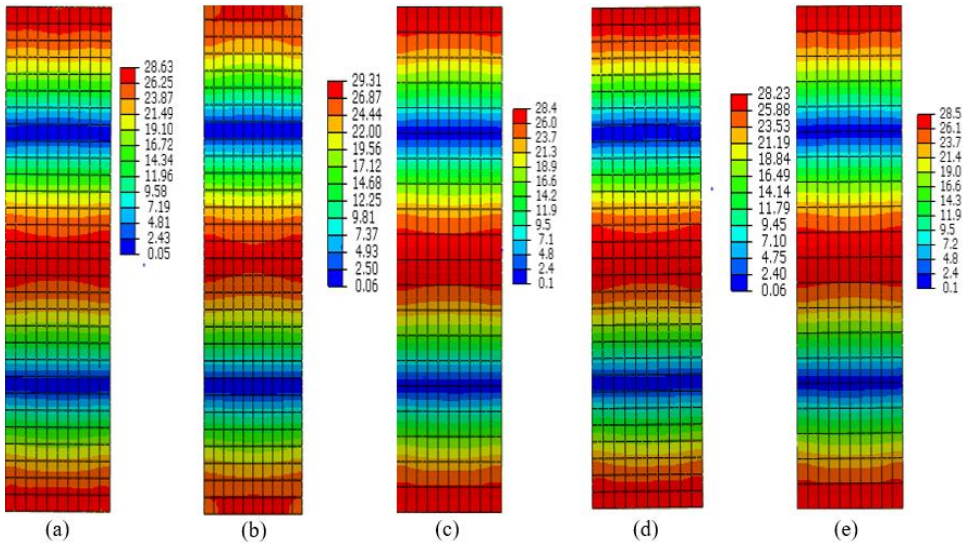

Fig. 6: Stress distributiom for partial load from both edge for θ = (±90°)s:(a) c/b = 0.1,(b) c/b =0.2, (c) c/b =0.3, (d) c/b =0.4, (e) c/b = 0.5.

As seen in the above figures, it may be due the fact the region of maximum stress occurs around the central part of the column, the column is expected to yield least buckling resistance as the stiffness of the panel is very less in that portion and there is only slight variation in the pre-buckling stress and the critical load that occurs at the middle portion of the column where the stress is maximum as observed in Fig 6 (a) to (e), whereas in column subjected to partial load from one edge the stresses are concentrated towards the edge of column when c/b = 0.1 wherein the stiffness of column is comparably less and these stresses are becoming uniform throughout the width of column when c/b approach towards the centre, i.e., c/b = 0.5.

6.2 Effect of position of concentrated edge load.

The effect of concentrated load from one and both sides of a slender column retrofitted with different ply-orientation varying from $\theta \approx (\pm 0°)$s to (±90°)s with a laminate thickness of 2mm on each face of column on the stability behaviour of partial loaded column for C-C edged conditions are depicted in Fig 7(a) and (b).

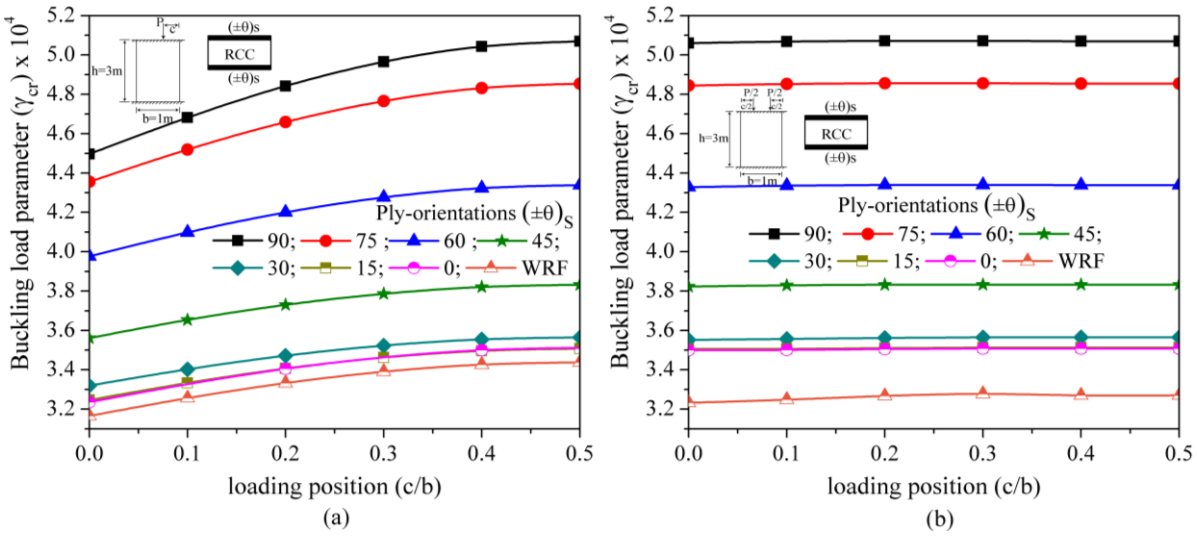

Fig 7: Variation of buckling load (γ_{cr}) with the position of (a) point load from one edge (b) point load from both edges.

In this analysis load width ratio of c/b = 0.1 to 0.5 was considered, intensity of load considered is 1000 N and kept constant for partial and concentrated load. As seen in Fig 7(a) and (b) variation of bucking load and stress distribution is similar and depicts same variation as partial load as in Fig. 4(a) and (b). One can observe from the Fig. 4(a) and (b) and Fig 7(a) and (b) that the buckling characteristic of column with concentrated load is similar to that of column with partial or strip load. Therefore, whatever the explanation given for Fig 4(a) and 4(b) is also holds good for Fig 7(a) and (b). Therefore it can be concluded from the above results that for analysis of column when subjected to partial in-plane edge load or concentrated load, it generates same results and similar type of stress distribution. So from results it is concluded that partial load is used for the study here onwards.

6.3 Effect of height of column.

The effect of height of column on the buckling behaviour with changing in c/b ratio from 0.1 to 0.5 with a ply-orientation of $\theta \approx (\pm 90°)$s has been studied in Fig 8(a) and (b) for partial load acting from one edge and from both edges respectively.

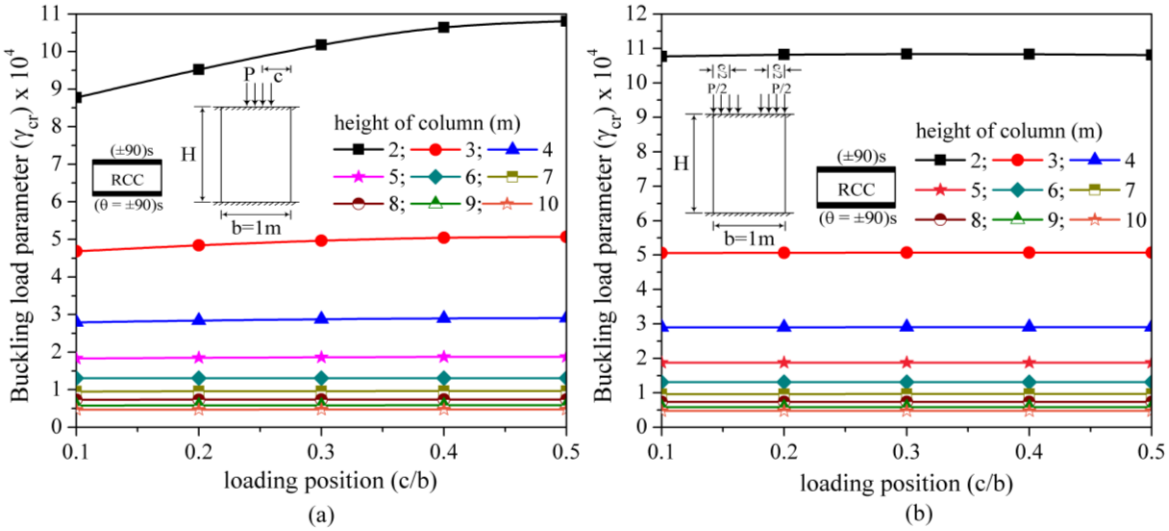

Fig 8: Variation of buckling load (γ_{cr}) for different height (H) with the position of (a) partial load from one edge (b) partial load from both edges.

As observed in Fig 8(a) buckling load increases as the c/b ratio increases and it is found to be maximum when c/b = 0.5 and maximum variation is seen for 2m height column and as the column height is increased variation in buckling load can be seen upto 4m, and thereafter when the height of column is increased form 5m to 10m there is no significant variation in the buckling load even with the increase of c/b ratio, it is worth mentioning that the buckling load more or less remains constant for column with height form 7m to 10m. There is approximately 90% decrease in the buckling load from 7m height column as seen in Fig 8(a). But whereas for column subjected to partial load from both edges as in fig 8(b), the variation in the buckling load pattern is similar to Fig 8(a), but in Fig 8(b) the buckling load variation for different c/b ratio from 0.1 to 0.5 is similar for all specified height of column. In both cases as the height of column is increased the stress distribution varies and is higher for short column and it is concentrated more at the centre. And the stress concentration decreases as the height of column increases eventually the buckling load also gets decreased because the stiffness of the column decreases.

7. Conclusions

The results from the analysis of slender thin walled column on buckling behaviour with retrofitting subjected to partial and concentrated edge loading in the plane can be summarized as follows:

1. The ply-orientation plays a significant part in the retrofitted column buckling strength. The

bucking strength of the column also improves as the ply orientation increases and found to be maximum at $\theta = (\pm 90°)_s$ and minimum at $\theta = (\pm 0°)$.

2. The loading position also plays a vital role in the column's buckling strength. The buckling load increases with the increase in the load position (c / b) and is observed to be minimum at c / b = 0.1 and maximum at c/b = 0.5 when loaded from one edge and found to be symmetry beyond c/b = 0.5. But it is not so in the case of loading from both edges, where the variation in the buckling load is almost negligible in the load position.

3. Around 47% is the maximum increase in buckling load when the column is retrofitted with $\theta = (\pm 90°)_S$ ply-orientation as compared to that of the column without retrofitting whereas it is only 2% in case of $(\pm 0°)_S$ ply-orientation.

4. The buckling strength of columns depends on many parameters, in which the height of the column governs major role. In case of short column the buckling load is greater eventually when the height of column is increased the stiffness gets decreased.

5. It can be noted that boundary condition play a main role on the buckling strength of column. It is found that for any given ply-orientation, the C-C edge column provides maximum buckling load relative to other boundary conditions.

References

1. Hadi, M. N., & Widiarsa, I. B. R. (2012). Axial and flexural performance of square RC columns wrapped with CFRP under eccentric loading. Journal of Composites for Construction, 16(6), 640-649.
2. Widiarsa, I. B. R., & Hadi, M. N. (2013). Performance of CFRP wrapped square reinforced concrete columns subjected to eccentric loading. Procedia Engineering, 54, 365-376.
3. Minafò, G., Monaco, A., D'Anna, J., & La Mendola, L. (2018). Compressive behaviour of eccentrically loaded slender masonry columns confined by FRP. Engineering Structures, 172, 214-227.
4. Elsanadedy, H. M., Al-Salloum, Y. A., Alsayed, S. H., & Iqbal, R. A. (2012). Experimental and numerical investigation of size effects in FRP-wrapped concrete columns. Construction and Building Materials, 29, 56-72.
5. Hadi, M. N. S. (2006). Behaviour of FRP wrapped normal strength concrete columns under eccentric loading. Composite structures, 72(4), 503-511.
6. Belouar, A., Laraba, A., Benzaid, R., & Chikh, N. (2013). Structural performance of square concrete columns wrapped with CFRP sheets. Procedia Engineering, 54, 232-240.
7. Charalambidi, B. G., Rousakis, T. C., & Karabinis, A. I. (2012). Finite element modeling of reinforced concrete columns seismically strengthened through jacketing seismically strengthened through partial FRP jacketing. criterion, 2(1).
8. Hales, T. A., Pantelides, C. P., & Reaveley, L. D. (2017). Analytical buckling model for slender FRP-reinforced concrete columns. Composite Structures, 176, 33-42.
9. Jiang, T., & Teng, J. G. (2012). Theoretical model for slender FRP-confined circular RC columns. Construction and building materials, 32, 66-76.
10. Chellapandian, M., Prakash, S. S., & Rajagopal, A. (2018). Analytical and finite element studies on hybrid FRP strengthened RC column elements under axial and eccentric compression. Composite Structures, 184, 234-248.
11. Mosallam, A., Allam, K., & Salama, M. (2019). Analytical and numerical modeling of RC beam-column joints retrofitted with FRP laminates and hybrid composite connectors. Composite Structures, 214, 486-503.
12. Sahu, S. K., Prabhakar, D. L., & Datta, P. K. (2001). Vibration and buckling of laminated composite plates subjected to non-uniform in-plane edge loading. Journal of Structural Engineering, 28(2), 75-80.
13. Nali, P., & Carrera, E. (2013). Accurate buckling analysis of composite layered plates with combined thermal and mechanical loadings. Journal of Thermal Stresses, 36(1), 1-18.
14. Tseng, Y. P., & Chou, L. C. (1993). Free vibration of orthotropic laminated plates according to partial hybrid plate

element. Journal of the Chinese Institute of Engineers, 16(1), 135-143.
15. Kishore, M. H., Singh, B. N., & Pandit, M. K. (2011). Nonlinear static analysis of smart laminated composite plate. Aerospace Science and Technology, 15(3), 224-235.
16. Whitney, J. M., & Riley, M. B. (1966). Elastic properties of fiber reinforced composite materials. Aiaa Journal, 4(9), 1537-1542.
17. Halpin, J. C., & Tsai, S.W. (1969). US Air Force materials laboratory report, AFML-TR. 67.
18. Selvadurai, A. P. S., & Nikopour, H. (2012). Transverse elasticity of a unidirectionally reinforced composite with an irregular fibre arrangement: Experiments, theory and computations. Composite Structures, 94(6), 1973-1981.
19. Hashin, Z., & Rosen, B. W. (1964). The elastic moduli of fiber-reinforced materials. Journal of applied mechanics, 31(2), 223-232.
20. Rajanna, T., Banerjee, S., Desai, Y. M., & Prabhakara, D. L. (2016). Effects of partial edge loading and fibre configuration on vibration and buckling characteristics of stiffened composite plates. Latin American Journal of Solids and Structures, 13, 854-879.